JEE Journal of Ecological Engineering

Journal of Ecological Engineering 2024, 25(7), 163–177
https://doi.org/10.12911/22998993/188081
ISSN 2299–8993, License CC-BY 4.0

Received: 2024.04.21
Accepted: 2024.05.16
Published: 2024.06.01

Surface Urban Heat Islands in Belo Horizonte, Manaus, Salvador Bahia Using Remote Sensing and the Weather Research and Forecasting Modeling

Julio Angeles Suazo[1*], Georgynio Rosales Aylas[2], Jose Luis Flores Rojas[3], Roberto Angeles Vasquez[4], Carmencita Lavado-Meza[5], Leonel De la Cruz-Cerrón[6], Nataly Angeles Suazo[7], Hugo Abi Karam[8], Davidson Martins Moreira[9]

[1] Universidad Nacional Autónoma de Tayacaja Daniel Hernandez Morillo, Escuela Profesional de Ingeniería Forestal y Ambiental, Tayacaja, Perú

[2] Universidade Federal do Espirito Santo, Department of Environmental Engineering, Vitoria, ES, Brazil

[3] Instituto Geofísico del Perú, Calle Badajoz, 169, 15498 Urb. Mayorazgo IV Etapa, Ate, Lima, Perú

[4] Universidad Nacional del Centro del Perú, Facultad de Ingeniería Civil, Huancayo, Perú

[5] Universidad Nacional Intercultural de la Selva Central Juan Santos Atahualpa, Escuela Profesional de Ingeniería Ambiental, Chanchamayo, Perú

[6] Universidad Continental, Facultad de Ingeniería, Huancayo, Perú

[7] Universidad Tecnológica del Perú. Facultad de Ingeniería de Sistemas, Av. Circunvalación 449, 12002 El Tambo, Huancayo, Perú

[8] Instituto de Geociências, Departamento de Meteorologia, Universidade Federal do Rio de Janeiro, Rua Athos da Silveira Ramos 274, Cidade Universitária, Ilha do Fundão, 21.941-916, Rio de Janeiro, RJ, Brasil

[9] Centro Universitario Senai Cimatec, Salvador, Brazil

* Corresponding autor's e-mail: julio_as_1@hotmail.com

ABSTRACT

The formation of urban heat islands is one of the effects related to urbanization, as it directly affects thermal comfort. There are several methodologies for its estimation, we can highlight the Gaussian (the best known), whose limitation focuses on the analysis of Gaussian surfaces. When the surface presents cases of poly-nucleated conglomerates, another type of approach (non-Gaussian) is recommended, such as the Quantile method. Therefore, this work seeks to estimate the intensity of surface urban heat islands (SUHI) in the long term (2001–2016) with both methodologies (Gaussians and Quantiles). Based on satellite data and the Weather Research and Forecasting (WRF) meteorological simulation, both with a special resolution of 5 km, for the metropolitan areas of Belo Horizonte, Manaus and Salvador, located in Brazil. Both methods indicate the formation of intense heat islands in the hottest months in the 3 cities studied, with less monthly variation compared to the surface temperature of the Earth's surface.

Keywords: surface heat island, megacities, Brazil, WRF.

INTRODUCTION

Urbanization processes modify the energy balance, since the darker the body, the greater the radiation absorbed; this process affects the surface and atmospheric energy balance. In urban areas, radiation from the sun accumulates on the surface more intensely, compared to rural areas. The accumulated energy is released, also intensely, and propagates in the atmosphere, impacting the upper levels, thus initiating the so-called forced convection processes [1, 2]. This configuration denotes an urban heat island (UHI), in which temperature changes are a product of human activities [3, 4]. With marked characteristics in mid-latitude cities, such as the formation of urban microclimates that

are warmer than their surroundings [5–7]. Being of importance since this differentiated local warming (urban-rural) can increase the intensity and frequency of extreme precipitation events [8, 9], as it favors atmospheric turbulence and intensifies precipitation events. The surface urban heat island (SUHI) can be defined as the relative warming of the surface temperature and is present both day and night [10]. This phenomenon is more evident in cities with removed or changed forests, as it causes an increase in temperature, perceived especially in city centers. To study the formation of the SUHI, the calculation of the SUHI footprint is usually used (influenced by urbanization and local climate). However, the SUHI footprint is not a determining factor, since in some cases it leads to erroneous conclusions [11]. For this reason, it must be accompanied by the calculation of SUHI intensity (SUHII), which describes the difference between urban and suburban temperatures.

The relative thermal contributions influencing SUHI formation are difficult to quantify. Well, generally only records from surface stations are available, which have limited representation. This is because the urban surface is constantly modified and this is reflected in the release of anthropogenic heat [11]. To understand the formation processes of SUHI, some researchers use various techniques such as the use of meteorological models, such as the WRF. Since, it makes possible the investigation of the impacts of urbanization on weather and climate. For example, the Weather Research and Forecasting (WRF) Urban Canopy Coupling Model (UCM) was developed as a tool to study urban environmental problems [12–16], even understand the impact of urbanization on temperature over long periods [17]. This makes it possible to study other phenomena, such as the formation of heat islands, such as that carried out for Singapore, a city with a tropical climate where the UHI can reach 5 °C [18].

Another way to study heat islands is by using satellite data. Like the one made by [19] who based their study on measurements of spectral albedo, thermal emissivity and radiative surface temperatures, recorded by the moderate resolution spectroradiometer (MODIS). As soon as, [20] uses this database to investigate the formation of SUHI for continental areas. Another form of objective application of MODIS satellite data is the study related to the formation of SUHI and its relationship with the load of atmospheric aerosols and vegetation cover [21]. The advantage of this database is due to the fact that it is robust data, since the tropical region has abundant cloud coverage, which impairs the continuous acquisition of quality data. Thus, its use is possible for the study of SUHI in mega-cities with tropical climates [22–28], adequately representing diurnal and nocturnal variations [3, 29]. The majority of Brazilian states are located in the tropical region. Given the territorial extension of this country, it is possible to find very noticeable topographic and climatic variations, which also affect local environmental conditions. As indicated by [10], the increase in temperature is influenced by roughness, soil occupation, permeability, physical properties of the materials, among other factors. One of the main cities of the Amazon, Manaus, a metropolitan area with an equatorial climate, is a humid region with high temperatures. It presents high intensities of diurnal UHI with a trend of 0.33 °C increase per decade. While cities such as Belo Horizonte and Salvador (with a tropical altitude and coastal climate, respectively) with similar UHI intensities, present a less intense increase trend, 0.23 °C and 0.14 °C per decade, respectively [30].

Of the traditional ways of estimating the SUHII, the Gaussian method stands out, proposed by [31], which fits the SUHI to a Gaussian surface. [31] shows that this method turns out to be versatile, especially when it comes to mega city studies. Surface heat islands in mega cities have greater interannual amplitude, due to the growing expansion of their suburban regions [32–34]. On the other hand, [25] suggests the Quantile method, based on the analysis of the median and the 95th quantile. This methodology is based on the fact that the urbanization processes of many cities have been inappropriate or not very homogeneous, which contributes to the formation of dispersed heat nuclei in cities. In this sense, the objective of this work is to estimate and verify the importance of the method used to estimate the SUHI intensity calculation. During the period of time, between 2001 and 2016, especially interested in the metropolitan areas of Belo Horizonte (MAB), Manaus (MAM), Salvador (MAS). For this, the Gaussian and Quantile methodologies proposed by: [31] and [25] respectively, based on data acquired from the MODIS satellite and results from the WRF model.

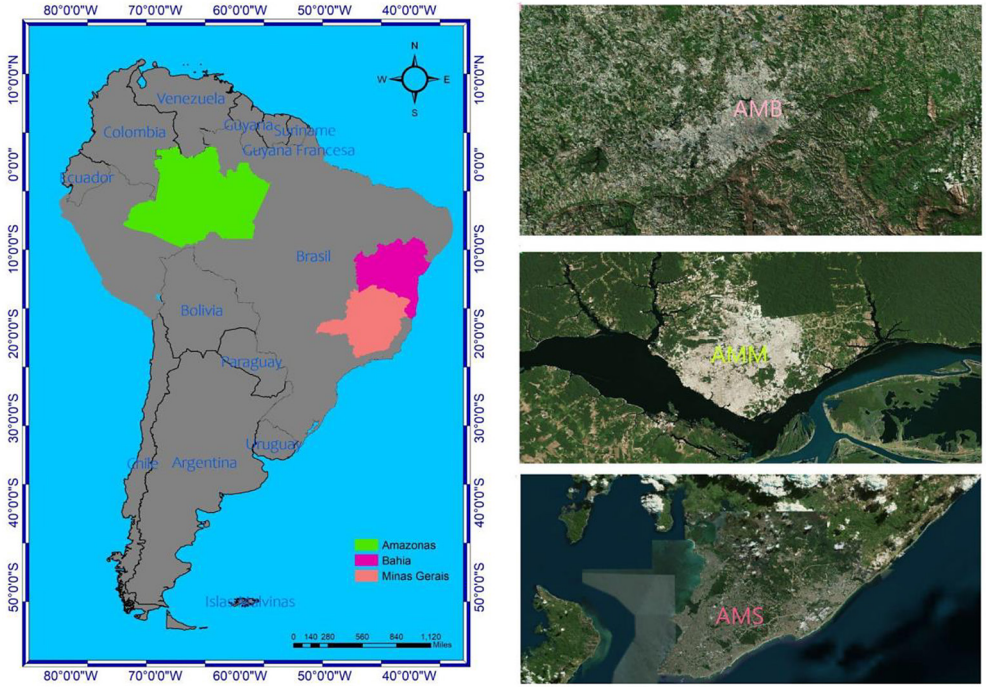

Figure 1. Brazil localization in South America, over the map are the states of the studies areas color different with. Satellite image of each metropolitan studying areas: AMB (southeast), AMM (north), AMS (northeast)

MATERIALS AND METHODS

Study site

The study regions are located in Brazil, as shown in Figure 1, from which 3 different regions stand out, southeast (AMB), north (AMM) and northeast (AMS).

The Brazilian city of Belo Horizonte is located at latitude -19.92, longitude -43.94, with an average altitude of 760 meters above sea level. Of rugged relief, it presents the highest altitudes in its southern end, reaching a maximum altitude of 1506 m. The characteristic climate of this Brazilian state is humid subtropical, hot and temperate, with abundant rainfall more intense in summer than in winter. Also, there are two well-defined seasons in Belo Horizonte due to the influence of air masses from mid-latitudes and tropical [35]: dry/cold season (April to October) and rainy/warm season (November to March). In the dry season (winter), the area is predominantly influenced by the atlantic polar front (APF), the south Atlantic subtropical area anticyclone (SASA), and the Atlantic polar anticyclone (across the Atlantic polar mass). The amount of precipitation and RH in the rainy season is expected. In general (according to the last ten years of recorded data), the prevailing wind in the directions in the region are NE to SE; the annual mean wind speed and temperature is 2.6 m/s and ~22 °C (range between 9 °C and 34 °C), respectively. Mean annual atmospheric pressure is ~920 mbar and mean annual RH is ~60%, with lower values in July, August and September. Precipitation rates are typically >50 mm/h in the summer, and become moderate and light (<3 mm/h) in spring/autumn and winter, respectively, with ~100 total rainy days per year. Meteorological information according to [36] at 10 and 40 m above ground levels from October 2019–September 2020. During this period, E to SE winds predominated, with a mean wind speed of 2.4 m/s. Higher temperatures (mean value: 23.1 °C) and precipitation amount (total = 1,817.4 mm) were recorded in the wet season (November-March) compared to the dry season (mean temperature of 21.1 °C and precipitation amount of 216.4 mm), although surprisingly high temperatures were recorded in September and October (mean value of these months = 24.5 °C). The highest daily rainfall volumes (>100 mm/d) were recorded in January, well above the annual average for the region. Rainfall events had a duration of ~3–4 days, starting with low rainfall intensity that gradually increased and decreased during the last day.

The Brazilian city of Manaus is located at latitude -3.12, longitude -60.03 and mean altitude of 100 m, with characteristic relief of plains. The

climatological behavior of this region has 2 distinct seasons, dry season from June to October and rainy season from November to May. The average annual temperature and precipitation are 26.78 °C and 2277 mm, respectively [37] and the accumulated precipitation was 412.8 mm; with temperature values in the hottest month (September: 28.3 °C) and the coldest month (February: 26.7 °C) (Auler et al., 2020; Yu Media Group, 2020). The predominant wind direction in Manaus is from the east-northeast, with diurnal variations due to breeze circulations [38].

Salvador, a Brazilian city in the northeastern region of Brazil, is located at latitude -12.97, longitude -38.47 and average altitude of 8 meters. Its characteristic geography is geographically constituted by narrow valleys and plains. The rainy period in this region occurs between March and July, in general the temperature has little variation, however, the average temperature decreases during the period of heavy rains. The meteorological characteristics show a maximum air temperature of 33.18 °C and a minimum of 25.54 °C (period 1980–2019) [39].

MODIS sensor

Carried by the TERRA and AQUA satellites, the MODIS sensor was launched into orbit in 200 and is managed by the National Aeronautics and Space Administration (NASA). The TERRA satellite provides information about the Earth's surface in wavelengths that include the visible and near-infrared spectra distributed over 36 bands [25].

MODIS thermal infrared (MODIS TIR) channels measure radiation from the top of the atmosphere (TOA), from which brightness temperatures can be derived using Planck's law. Land surface temperature (LST) level 2 and 3 are contained within the MOD11 product, with spatial resolution of 1 km and 5 km under clear sky conditions. Land surface temperature (LST) data are corrected using day-night TIR data pairs grouped into seven bands, without knowing the water vapor and atmospheric temperature profiles with high accuracy [40]. In addition, in order to generate more regionally representative urban temperature estimates, the three-dimensional roughness of urban surfaces, whose scale depends on satellite images, is considered [10].

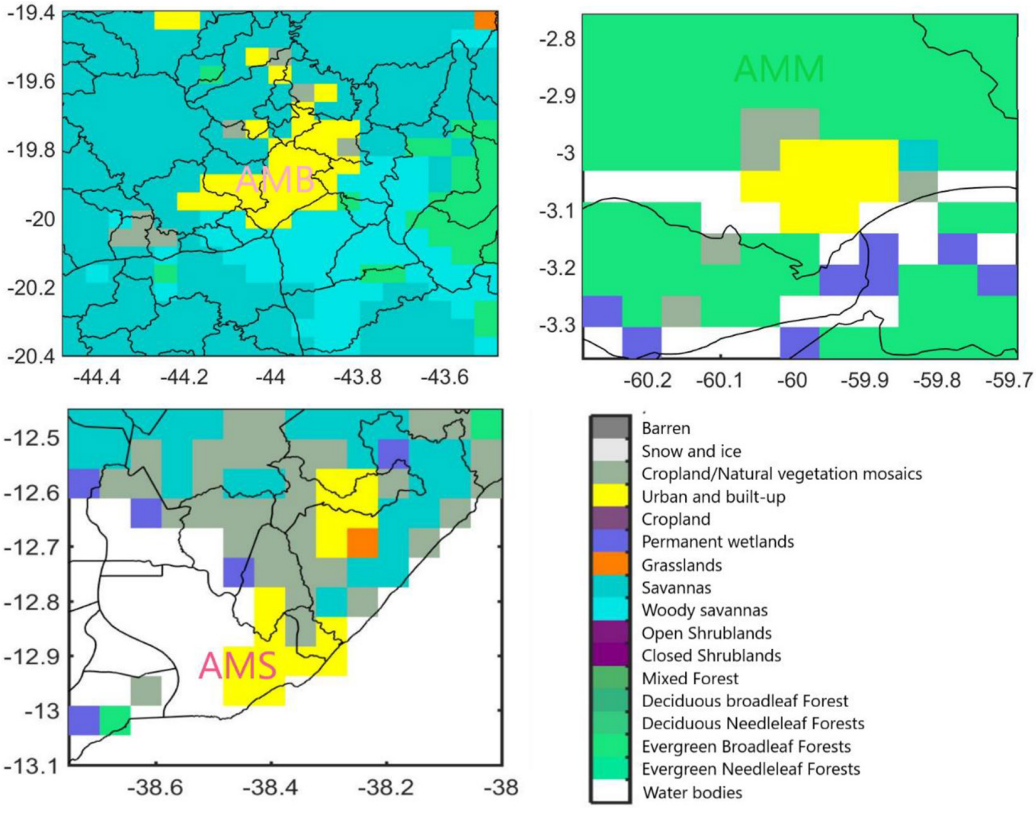

Figure 2. Land cover classes for the 3 study areas (AMB, AMM and AMS), according to the IGBP classification, for the period of December 2006

The identification of land cover types, with which we were able to identify urban and rural land cover. This information was verified with the parameters established by the International Geosphere-Biosphere Project (IGBP), on the MCD12C1 MODIS land cover classes (resolution 0.05°), which served as a baseline for the identification and delimitation of urban and rural areas and the delimitation of the corresponding borders. This project identifies 17 land cover classes defined by the IGBP [41] (example, [23–25, 42–45], whose results can be observed in Figure 2.

The satellite data used in our study, with a resolution of 5 km, provides a valuable overview of urban heat island (UHI) patterns across the study areas. However, due to the intricate urban complexity and diverse topography of these regions, there are limitations in capturing microclimatic variations within smaller urban zones [46–48]. The 5 km resolution may overlook significant microclimatic variations, particularly in areas with heterogeneous land cover and urban structures. These localized variations can be influenced by factors such as building density, land use patterns, topography, and vegetation cover, which might not be fully captured at this spatial scale [49]. While our study aims to provide a comprehensive analysis of UHIs at a broader scale, it's essential to recognize the potential limitations when extrapolating these findings to smaller urban areas within the studied cities, as highlighted by different research groups [50–52]. Future research using higher spatial resolution satellite data or incorporating ground-based measurements could offer more detailed insights into these microclimatic variations, thereby enhancing the accuracy and reliability of UHI assessments in complex urban environments [53].

Thermal characteristics

The LST data are available on the MODIS satellite web page with a spatial resolution of 5 km. The thermal amplitude was calculated from the difference between the temperature value at

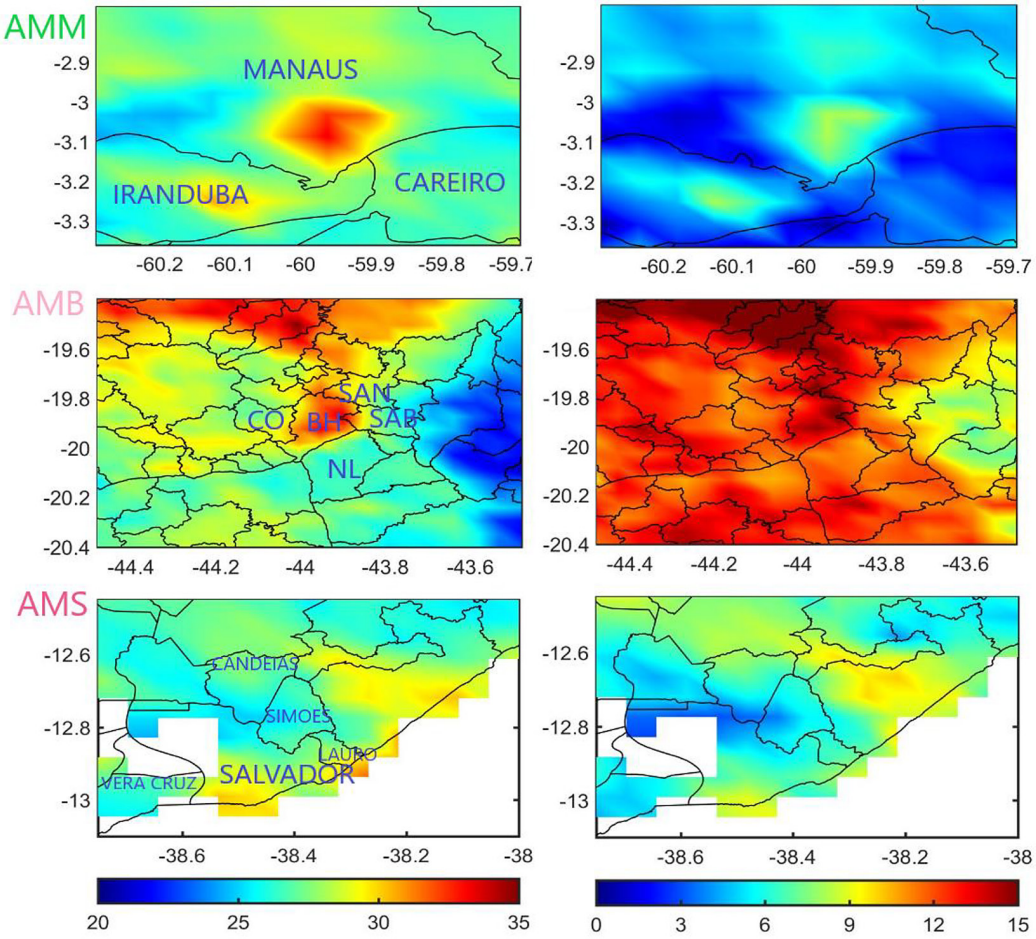

Figura 3. Representation of LST, on the left the surface temperature distribution, on the right the thermal amplitude. In both cases the figures represent the average from 2001 to 2016

each point in the study area minus the minimum value found in the LST. The surface surface temperature (LST) and thermal amplitude, for each study region, are shown in Figure 3. As shown in Figure 3, the SMA is the region with the highest temperature among the three regions considered in this study. In the WMA we can find thermal amplitudes of up to 15 °C, while the maximum temperatures are concentrated in the central urban region. Similarly, this characteristic is repeated for the other metropolitan areas. However, the AMS region shows areas of maximum temperatures (35 °C) outside the capital, due to the fact that the densest groups of buildings are scattered and are formed around the industrial poles. The geographical situation of Salvador, located between the coast of the Atlantic Ocean and the Bay of Todos os Santos, presents less variation in thermal amplitude. This situation is caused by the trade winds, which guarantee an exchange of air masses and help to cool the city. Therefore, the formation of heat islands is more complex than in other cities.

The monthly LST variations for AMB, AMM and AMS, Figure 4, show the diurnal and nocturnal evolution, for 3 regions of each metropolitan area: urban, border and rural. Being surrounded by rock formations AMB (Figure 4a), acts as a natural barrier to airflow and makes heat dissipation less intense. LST in the AMB is more intense during the warm months. The month of greatest intensity is October, with temperatures reaching 34 °C in the interior of the rural area, the border region (urban-rural) reaching 29 °C and the rural region reaching 30 °C. Being surrounded by mountain ranges, heating can be less varied in the cold months. This condition is especially observed in June, the month with the lowest thermal amplitude; thus, the central urban region has 25 °C, the border region 23 °C, and the rural region 22 °C. During the night period, the temporal evolution of the LST presents similar amplitudes for all locations. The maximums were found in January, central urban region with 21 °C, border with 20 °C and rural with 18 °C; while the minimum was found in July, where the urban center reaches 15 °C, border 14 °C and rural 11 °C.

The LST for the WMA, the maximum found for each region, urban center, border and rural, are 31 °C, 28 °C and 28 °C, respectively, during the month of August. The minimums found are in February, where the urban center, border and rural areas have 25 °C, 24 °C and 24 °C, respectively. The mean LST during the night period, has maximums in October for the urban centers, frontier

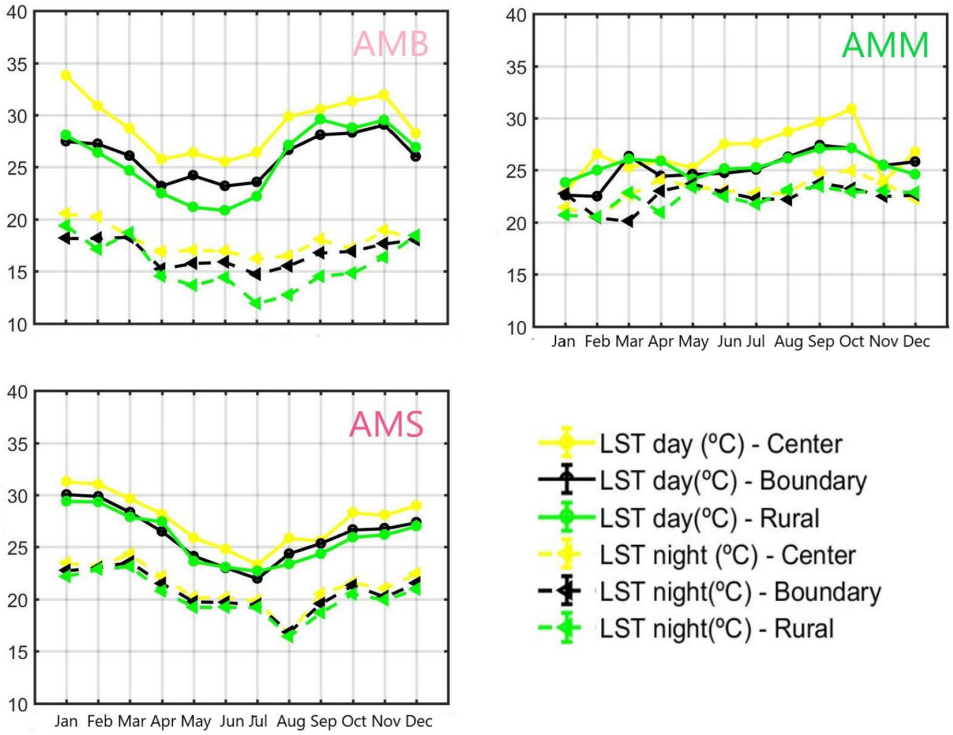

Figure 4. Temporal evolution of LST for the 3 study areas, in the daytime and nighttime periods. In the graphs we can distinguish 3 regions within each study area: the urban center, urban and rural border

and rural areas, with temperatures of 25 °C, 24 °C and 24 °C, respectively. Even in the night period, the minimums are observed in March, where the urban centers have 21 °C, the frontier 21 °C and the rural area 22 °C.

The maximum LST is observed in December for the urban area 30 °C, border 28 °C and rural 28 °C. The minimums are observed in June for all localities, urban center 25 °C, border 24 °C and rural 24 °C. During the night period, the temporal evolution of the LST has maximums in January for urban (24 °C), border (23 °C) and rural (22 °C) centers. The minimums are observed in August for the urban (18 °C), border (17 °C) and rural (17 °C) areas.

WRF meteorological model

The Weather Research and Forecasting (WRF) model, a meteorological forecasting model, was used to simulate the behavior of surface temperature. The initial conditions for the simulations were defined from synoptic-scale meteorological data. This database is available at the web address https://rda.ucar.edu/, from which the NCEP-GFS data were taken, with a spatial resolution of 0.25° (27–28 km) and a time interval of 6 hours. In the case of geographic data, the MODIS database of the United States Geological Survey (USGS), available as standard on the model's website, was used.

The following combination of parameterizations was used in the development of this work: the Betts - Miller - Janjic cluster scheme and the Mellor - Yamada - Janjic (MYJ) planetary boundary layer, both proposed by [54]. Formulated to try to solve precipitation simulation problems, which were sometimes widely scattered over the oceans, so, it introduces the "cloud efficiency" method to provide an additional degree of freedom in determining the heat and moisture fate profiles. The WRF Double Moment 5 and 6 class micro-physics scheme, allows flexibility in variable raindrop size distribution, predicting cloud number, precipitation amount and explicit organization of condensation nuclei [55]. The RRTMGU shortwave and longwave radiation scheme, a new version of RRTM, includes the MCICA method of random cloud superposition [56]. With this information, WRF simulations were performed with a spatial resolution of 5 km and a temporal resolution of one hour, from which the calculations were made.

Given the vast size and quasi-continental characteristics of the country, simulating its different territorial units represents a significant challenge. Although the country's climate is predominantly tropical, there is notable climatic variability across its territory. Therefore, the selection of parameterizations for this study was complex, considering that not all configurations are suitable for each locality, which led to the decision to base the parameterizations on those used by CPTEC. However, not all parameterizations work for the studied locations. Priority was given to maintaining the stability and continuity of the simulations without excessively sacrificing their accuracy. For cumulus parameterization, Betts-Miller-Janjic was chosen for its numerical stability and effectiveness in tropical regions where deep convection is common, which can be used for our study areas. For the planetary boundary layer, MYJ was selected due to its ability to accurately represent local turbulence and rapid transitions thereof. The WRF double moment 5 and 6 class schemes can simulate a wide range of meteorological conditions and cloud types, from deep convective clouds to stratiform clouds. The rest of the parameterizations follow those defined by CPTEC.

The WRF model faces challenges when simulating wind fields, requiring a thorough and detailed exploration of suitable parameterizations. However, it performs well in modeling temperature fields, even at high spatial resolutions, suggesting that a spatial resolution of 5 km should not pose significant issues. Despite the viable alternatives of using urban schemes, these may have a moderate impact on very high-resolution simulations (500m) for variables such as 2-meter temperature or relative humidity as highlighted by [57]. This suggests that using this methodology with a spatial resolution of 5 km would likely be ineffective.

On the WRF model a spatial scale of 5 km, temperature simulation proves to be optimal at this resolution as found by [58]. It is possible to capture important processes that influence urban circulation, as this resolution allows for the observation of the seasonality of mesoscale and synoptic systems, as well as local microclimatic behavior. In places like Belo Horizonte, where no specific microclimatic system predominates, a higher resolution may be unnecessary, as studying the local microclimate requires more detailed and focused analysis on specific areas; consequently, no

direct impact is perceived across the entire urban region. On the other hand, in areas with frequent dual phenomena, such as Salvador, the most observed systems, the sea and land breezes, are adequately captured with a resolution of 5 km and are the main factors influencing urban ventilation in this area. In Manaus, two well-defined climatic periods are identified: one with regular rain in the afternoons and another in which mesoscale and/or synoptic systems trigger periods of intense rain that can last several consecutive days.

Gaussian and quantile method

The Gaussian adjustment method [31], of the special SUHII distribution and its purpose is to characterize the complete UHI in magnitude and spatial extent without the use of in situ measurements. This method is suitable for comparative studies of SUHI for several cities because the estimated quantity is not the absolute temperature, but the simultaneous temperature difference between urban and rural areas. This differentiation procedure partially eliminates the influences of meteorological conditions and other sources of error [22]. However, the method of [31] for estimating the intensity and spatial extent of SUHI has some drawbacks. For example, the rural LST field may not be correctly represented by a plane, also the use of higher spatial resolution data allowing the identification of smaller features would probably not make a Gaussian surface and, therefore, would require a re-scaling process. In addition, the method works well for cities with ellipsoidal shapes, but has problems for cities with different shapes [25], such as those developed around lakes and bays like the AMM and AMS as shown in Figure 1. Finally, in nighttime periods the SUHI intensity may decrease enough to no longer have a Gaussian shape, because urban and rural temperatures are sometimes very similar.

The Quantile method [25], is based on the statistical analysis of urban and rural region LST quantiles. Which points out the difficulty of Gaussian methods, which adjust the spatial distribution of UHI intensities so that the highest heat island intensities are centrally located. Thus, in the presence of multiple heat sources, it presents difficulties. In sum, the quantile method becomes robust because the calculations do not use the absolute temperature difference, but the simultaneous temperature difference between urban and rural areas.

The Gaussian method is commonly used to analyze spatial patterns and smooth out noise, while the Quantile method is effective in capturing extreme values and variability in the data. By employing these two methods in tandem, we aim to provide a comprehensive analysis of SUHII, capturing both its general spatial distribution and its extreme variations. However, it's important to note that each method has its limitations; Gaussian may oversmooth the data, while Quantile may be sensitive to outliers. In our study, we have attempted to mitigate these limitations through careful calibration and validation processes.

RESULTS

Daytime and nighttime SUHI

Case Brazil: Belho Horizonte, Salvador Bahia and Manaus

Figures 5 and 6 A, B and C show the scatter plots, between the methods (Gaussian and Quantiles) used for this work, for AMB, AMM and AMS. Secondly, for AMM in Figure 5B, the straight line fitting the data is equal to 1.06, the intercept is equal to -0.04 and the correlation index is equal to 0.47. For the AMS in Figure 5C, the straight line fitting the data is equal to 1.95, the intersection is equal to -2.43 and the correlation index is equal to 0.11. The best correlation is observed for the AMB, with a positive trend for both daytime and nighttime, indicating the agreement of the results found.

Likewise, in Figure 6A for the night time, the line that fits the data is equal to 0.94, the intersection is equal to 0.08 and the correlation index is equal to 0.74. In Figure 6B for the night schedule, the line that fits the data is equal to 0.44, the intersection is equal to 0.97 and the correlation index is equal to 0.10. In Figure 6c for the night schedule, the line that fits the data is equal to 0.61, the intersection is equal to 3.13 and the correlation index is equal to 0.07. The estimation made based on the WRF model calculations for all cases shows the tendency to overestimate the values. The calculation of SUHI with the quantile methodology, see Figures 7 and 8, most of the time the WRF can follow the behavior.

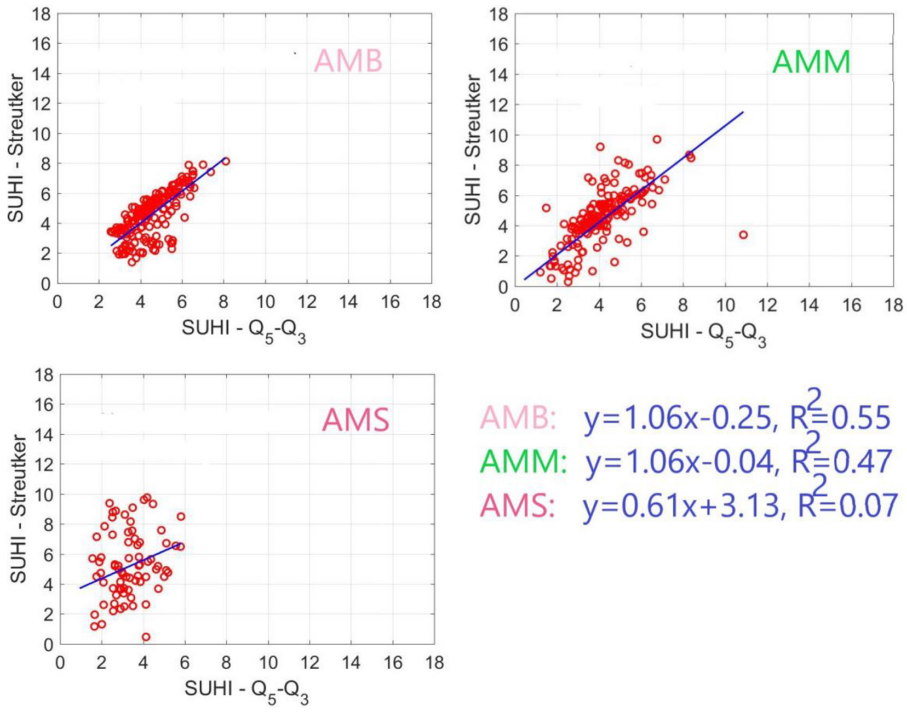

Figure 5. Scatter plot of diurnal SUSHI, obtained with the Streutker method vs quantiles, for the 3 metropolitan areas

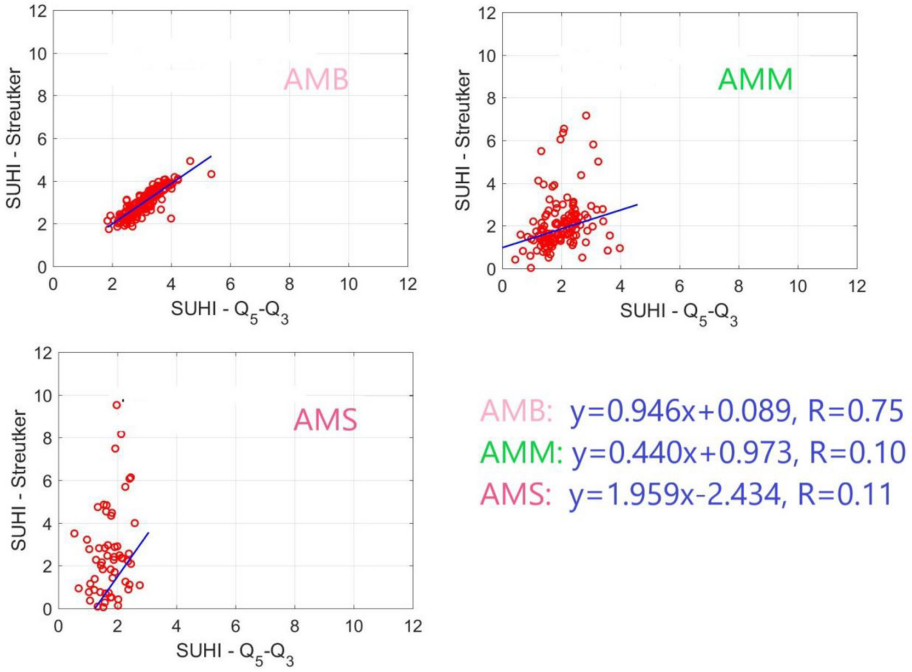

Figure 6. Scatter plot of nocturnal SUSHI, obtained with the Streutker method vs quantiles, for the 3 metropolitan areas

Surface urban heat island (SUHI)

The long-term average SUHI behavior (2001–2016) are shown in Figures 7 and 8. These figures organize the information so that SUHI values for day and night can be presented on a monthly basis. For this analysis we must consider that the diurnal interannual amplitude of SUHI has greater variation than the nocturnal, this is due to the effect of seasonal changes and its effect

on the change of vegetation cover, especially in rural áreas [33].

Figure 7 shows the results found for the AMB. Using the Gaussian method for the diurnal period, the extremes occur in the months of January and August, maximum and minimum respectively. With the quantile method for the diurnal period, the maximum month is in January and the minimum in July. The difference between maximum and minimum is about 4 °C and 2 °C, for the Gaussian and Quantile method respectively, which could be the effect of the influence of the seasons in the southern hemisphere (summer and winter). Being of similar intensity to that found by [49], who report mean UHI of 4.7 °C for the city of Belo Horizonte. On the other hand, see Figure 8, the nocturnal variations are smaller, highlighting that the maximum found (coincidentally) for both methods occurs in the same month (August) and the values found by both methods are very close. The formation of SUHI maxima in the AMB, day-night, is more than 2 °C, whose summed fluctuations exceed 2 °C, this behavior is repetitive in most of the warm months. On the other hand, the lowest day-night SUHI variation occurs in the month of July, where the variation is less than 0.1 °C for both methods, while the sum of their fluctuations can exceed 1 °C.

The SUHI for the WMA is presented in Figure 7. With the Gaussian method, the diurnal maximum occurs in a seasonal transition month (winter–spring) and the minimum occurs during the summer. The quantile method shows the same behavior as the Gaussian method. However, the Quantile method shows higher SUHI variation of about 3 °C (maximum - minimum) while the Gaussian method shows 2 °C. On the other hand, the SUHI Gaussian Figure 8, nocturnal maximum, occurs in the same month as those found by the diurnal maximum, the SUHI Quantile is advanced one month. On the other hand, the minimum occurs in a cold month (April–Autumn) for the Gaussian and the other during the transition of season change (December) [30]. For the diurnal UHI, Manaus recorded the highest value among all metropolises, with a mean intensity of +5 °C.

The diurnal-nighttime variation of Gaussian SUHI, in the WMA is greater than 3 °C, and the accumulated fluctuations exceed 4 °C. The smallest variations were found in February, being greater than 1 °C, whose summed fluctuations exceed 4 °C. The SUHI with the quantile method presents greater differences, exceeding 1.5 °C in most of the months. The calculation of the SUHI for the AMS, see Figure 7, with the Gaussian method, shows that the maximum diurnal SUHI formation

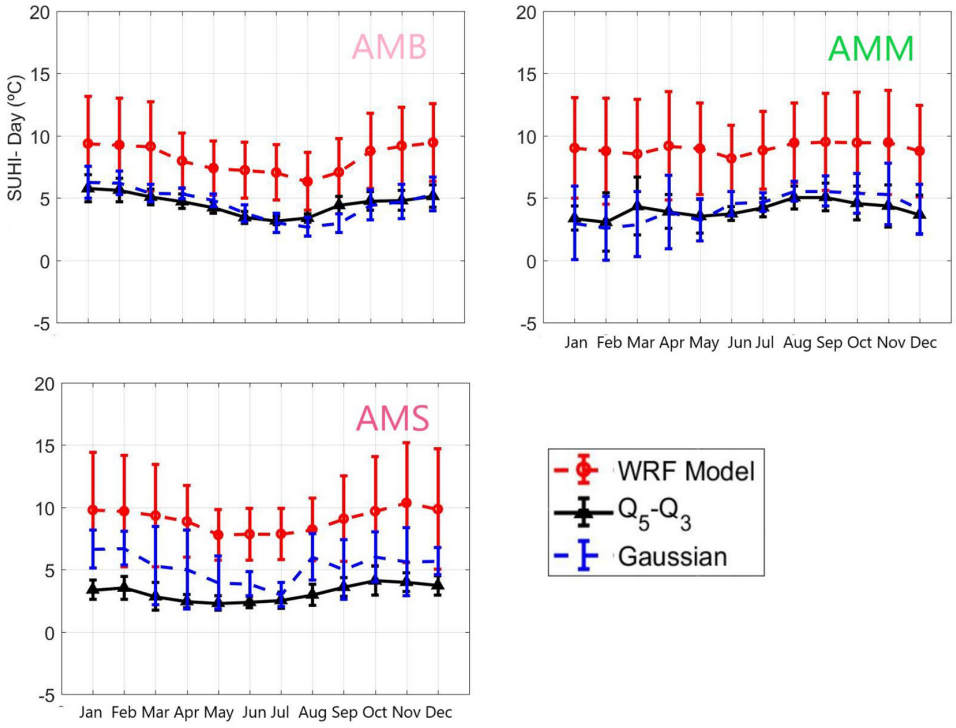

Figure 7. Monthly variation of SUSHI training in the different metropolitan areas, the monthly values correspond to the period from 2001 to 2016

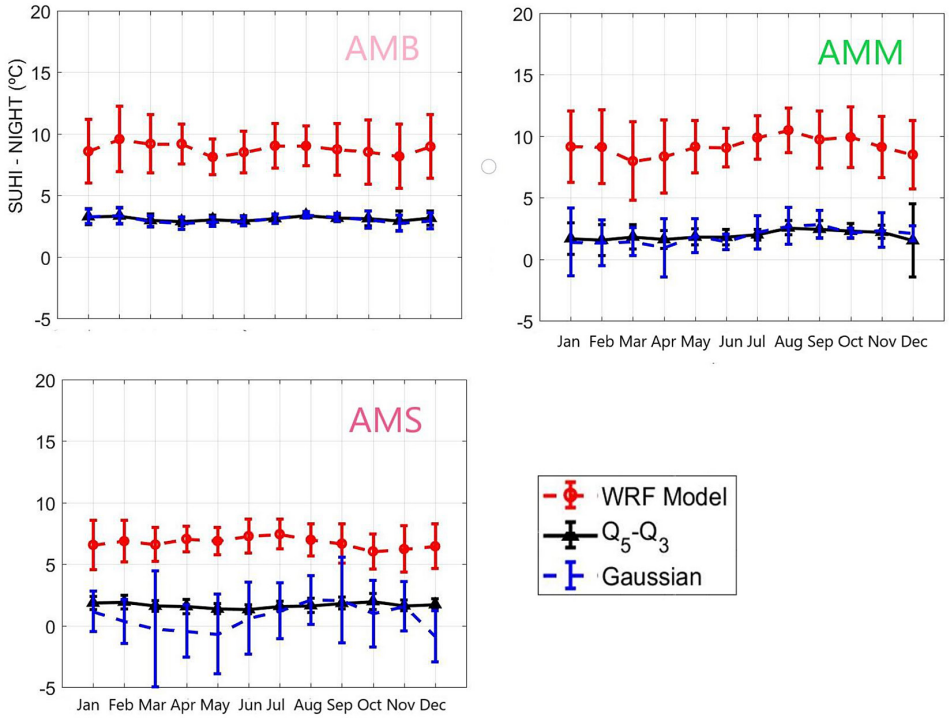

Figure 8. Temporal evolution of 2001–2016, monthly average nocturnal SUHI (°C) with their respective standard deviations using the quantile method, Streutker and WRF, for AMB, (b) AMM and (c) AMS.

occurs during the summer, while the minimum during the winter. The Quantile method shows totally different behavior, with the maximum in a winter month and the minimum in an autumn month. The difference between extremes with the Gaussian method is about 4 °C, for the Quantiles 2 °C. With respect to the night values, Figure 8, the Gaussian method changes diametrically the extremes (with respect to the daytime observation), the maximum being in a winter month and the minimum in an autumn month. With the quantile method, the formation of nocturnal SUHI, the maximum occurs in a spring month and the minimum in a transition month. The variations between the extremes for the nocturnal Gaussian are about 2 °C, while with the Quantiles the variation is a little more than 0.6 °C. The results of the WRF model for the analysis of the SUHI formation can be seen in Figures 7 and 8 (diurnal and nocturnal), for the AMB the diurnal and nocturnal maxima occur in spring and summer months. In the MMA the maxima are found in winter months and the minima in different periods, end of summer and winter. In the AMS the diurnal maximum occurs in a spring month and the minimum in an autumn month, while the nocturnal maximum occurs in a winter month and the minimum in spring. However, it is highlighted that for both periods (diurnal and nocturnal) the WRF estimates are usually higher than those found by the other methods, which is a common result, being that the estimates run by meteorological models usually over-estimate the predictions [50].

DISCUSSION

The SUHII found for the regions studied follow a quasi-seasonal behavior (Figure 7 and 8), which decreases with the arrival of the warm months. This indicates that the main SUHI centers are gaining intensity. Therefore, we can understand that the formation of SUHII, in addition to being directly influenced by urban and rural characteristics, is also affected by the phenology of the rural environment, since it can differ considerably between cities, even in the same climatic zone (Sismanidis et al., 2022). The presence of vegetation cover alters the thermal contrast, urban areas with high vegetation cover and water have lower thermal amplitude, as they have higher evapotranspiration rates, consequently altering sensible and latent heat fluxes, keeping the surface temperature cooler than in the border zone [3, 51]. Likewise, urban and population growth contributes to the increase in SUHI intensity, which

can reach values higher than 1.5 °C per decade (Monteiro et al., 2021). Therefore, the vulnerability of cities may be affected, given the intrinsic relationship formed between SUHI and local hydroclimatic conditions, such as the induction of local storms caused by urbanization.

The Brazilian cities studied do not show an exclusively homogeneous urban development, which is reflected by showing several nuclei of higher SUHI intensity (see Figure 2), however, there is always a predominant area. By presenting several high intensity cores, these could influence the representativeness of the final mean, since, SUHI estimation methods are not always sensitive enough to detect and include non-Gaussian forms, as highlighted by [24, 25, 52]. In this way, [53] stresses on the importance of the early study of urban geometry, since, it is the aspect that most contributes to the development of the UHI effect.

Thus, environmental and geographic factors are of great importance, since they can favor or obstruct local ventilation patterns, contributing to or retarding accelerated warming. Thus, albedo directly influences the temperature of the local atmosphere [54]. Urban ventilation is directly dependent on horizontal configuration, as it alters surface roughness and reduces heat dissipation by ventilation, while vertical configuration modifies SUHI by up to 30% [55]. Tropical cities are dependent on urban design and planning, as they modify ventilation factors. Urban ventilation is more efficient than extensive use of vegetation, water bodies or albedo modifications for air temperature, where there is already a high level of humidity [56].

CONCLUSIONS

The study of SUHI formation is a complex task, since it involves the study of several factors (environmental, climatic, geographic, population, among others). In this sense, we corroborated the existence of the formation of multiple areas of intense SUHI, and they are influenced by seasonal variation, being of lower intensity in winter and reaching their maximum levels in summer. In general, the region that presented the lowest surface temperature and consequently the lowest SUHI variation was the AMS, while the most affected region was the AMM.

It was possible to corroborate the feasibility of the quantile method, used as a method for estimating SUHI of non-ellipsoidal cities. Especially when the spatial resolution is so high that it does not allow a Gaussian surface adjustment or when the cities have more than one center of maximum surface temperature, or when the city has a border with water bodies. Therefore, it was important to couple the quantile method to the WRF model to calculate the SUHI, thus proposing future research to not only predict surface temperatures, since the WRF model will be able to estimate predictions of surface urban heat island intensities. Thus, detailed knowledge of urban heat islands, with their differences and specificities, are vital for the formulation of public health policies. Since, there is a relationship between SUHI formation and the intensity of meteorological events, as it directly influences the management of natural (heat waves) and anthropogenic (urban heat island) risks. Serving as a supply of information for the development of mitigation strategies for extreme events and disaster risks.

Our results indicate significant seasonal variations in SUHII across different regions. These findings have important implications for urban planning and public health in tropical cities. Seasonal variations in UHIs can impact energy consumption, air quality, and human health, particularly during extreme heat events. Urban planners and policymakers should consider these seasonal variations when developing strategies to mitigate the impacts of UHIs and improve urban resilience. For instance, in strategies to mitigate neglected Tropical Infectious Diseases such as Dengue epidemics.

Acknowledgment

Thank you Senai Cimatec Supercomputing Center "Yemoja" cluster, where we did the WRF simulations.

REFERENCES

1. Bahi H., Mastouri H., and Radoine H. 2020 Review of methods for retrieving urban heat islands," in Materials Today: Proceedings, 27, doi: 10.1016/j.matpr.2020.03.272.
2. Stewart I.D., Krayenhoff E.S., Voogt J.A., Lachapelle J.A., Allen M.A., and Broadbent A.M. 2021. Time Evolution of the Surface Urban Heat Island,

Earth's Futur., 9(10), doi: 10.1029/2021EF002178.

3. Li C., Zhang N. 2021. Analysis of the Daytime Urban Heat Island Mechanism in East China, J. Geophys. Res. Atmos., 126(12), doi: 10.1029/2020JD034066.
4. Song J., Wang J., Xia X., Lin R., Wang Y., Zhou M., Fu D. 2021 Characterization of urban heat islands using city lights: Insights from modis and viirs dnb observations. Remote Sens., 13(16), doi: 10.3390/rs13163180.
5. Oke T.R. 1987. Boundary layer climates, Second edition.
6. Dimoudi A., Kantzioura A., Zoras S., Pallas C., Kosmopoulos P. 2013. Investigation of urban microclimate parameters in an urban center. Energy Build., 64 doi: 10.1016/j.enbuild.2013.04.014.
7. Parece T.E., Li J., Campbell J.B., Carroll D. 2016. Assessing urban landscape variables' contributions to microclimates, Adv. Meteorol., 2016, doi: 10.1155/2016/8736263.
8. Climate and Disaster Resilience in Cities, Manag. Environ. 2011. Qual. An Int. J., 22(5), doi: 10.1108/meq.2011.08322eaa.012.
9. Joerin J., Shaw R. 2011. Mapping climate and disaster resilience in cities, Community, Environ. Disaster Risk Manag., 6, doi: 10.1108/S2040-7262(2011)0000006009.
10. Voogt J.A., Oke T. R. 2003. Thermal remote sensing of urban climates, Remote Sens. Environ., doi: 10.1016/S0034-4257(03)00079-8.
11. Zhou D., Zhao S., Zhang L., Sun G., Liu Y. 2015. The footprint of urban heat island effect in China, Sci. Rep., 5, doi: 10.1038/srep11160.
12. Holt T. and Pullen J. 2007. Urban canopy modeling of the New York City metropolitan Area: A comparison and validation of single- and multilayer parameterizations, Mon. Weather Rev., 135(5), doi: 10.1175/MWR3372.1.
13. Chen F. Kusaka H., Bornstein R., Ching J., Grimmond C.S.B., Grossman-Clarke S., Loridan T., Kevin W. Manning, Martilli A., Miao S., Sailor D., Salamanca F.P., Taha H., Tewari M., WangX., Wyszogrodzki A.A., Zhang C. 2011. The integrated WRF/urban modelling system: Development, evaluation, and applications to urban environmental problems, Int. J. Climatol., 31(2), doi: 10.1002/joc.2158.
14. Chen F., Yang X., and Zhu W. 2014. WRF simulations of urban heat island under hot-weather synoptic conditions: The case study of Hangzhou City, China, Atmos. Res., 138, doi: 10.1016/j.atmosres.2013.12.005.
15. Mohammed A., Khan A., Santamouris M. 2021. On the mitigation potential and climatic impact of modified urban albedo on a subtropical desert city, Build. Environ., 206, doi: 10.1016/j.buildenv.2021.108276.
16. Khodmanee S. and Amnuaylojaroen T. 2021. Impact of Biomass Burning on Ozone, Carbon Monoxide, and Nitrogen Dioxide in Northern Thailand, Front. Environ. Sci., 9, doi: 10.3389/fenvs.2021.641877.
17. Han L. Yu X., Xu Y., Deng X., Yang L., Li Z., Lv D., Xiao M. 2021. Enhanced Summertime Surface Warming Effects of Long-Term Urbanization in a Humid Urban Agglomeration in China, J. Geophys. Res. Atmos., 126(21), doi: 10.1029/2021JD035009.
18. Mughal M.O., Li X.X., Norford L.K. 2020. Urban heat island mitigation in Singapore: Evaluation using WRF/multilayer urban canopy model and local climate zones, Urban Clim., 34, doi: 10.1016/j.uclim.2020.100714.
19. Jin M., Dickinson R.E., Zhang D.L. 2005. The footprint of urban areas on global climate as characterized by MODIS, J. Clim., 18(10), doi: 10.1175/JCLI3334.1.
20. Cheval S., Dumitrescu A., Irașoc A., Paraschiv M.G., Perry M. and Ghent D. 2022.MODIS-based climatology of the Surface Urban Heat Island at country scale (Romania), Urban Clim., 41, doi: 10.1016/j.uclim.2021.101056.
21. Siddiqui A., Kushwaha G., Nikam B., Srivastav S.K., Shelar A., Kumar P. 2021. Analysing the day/night seasonal and annual changes and trends in land surface temperature and surface urban heat island intensity (SUHII) for Indian cities, Sustain. Cities Soc., 75, doi: 10.1016/j.scs.2021.103374.
22. Tran H., Uchihama D., Ochi S., Yasuoka Y. 2006. Assessment with satellite data of the urban heat island effects in Asian mega cities, Int. J. Appl. Earth Obs. Geoinf., 8(1), doi: 10.1016/j.jag.2005.05.003.
23. Angeles Suazo J.M., Flores Rojas J.L., Karam H. A., Arana Mallma G.R., Angeles Vasquez R.J. 2019. Isla de Calor Urbana Superficial en las Áreas Metropolitanas de Huancayo y Arequipa/Perú, Anuário do Inst. Geociências - UFRJ,.
24. Angeles J., Angeles R., Rojas J.L.F., Karam H. 2019. Estimación de Isla de Calor Urbana Superficial en el Area Metropolitana de Iquitos/Peru, Anuário do Inst. Geociências - UFRJ, 42(1).
25. Flores R.J.L., Pereira Filho A.J., and Karam H.A. 2016. Estimation of long term low resolution surface urban heat island intensities for tropical cities using MODIS remote sensing data, Urban Clim., doi: 10.1016/j.uclim.2016.04.002.
26. Carrillo-Niquete G.A., Andrade J.L., Valdez-Lazalde J.R., Reyes-García C., Hernández-Stefanoni J.L. 2022. Characterizing spatial and temporal deforestation and its effects on surface urban heat islands in a tropical city using Landsat time series, Landsc. Urban Plan., 217, doi: 10.1016/j.landurbplan.2021.104280.
27. Senevirathne D.M., Jayasooriya V.M., Dassanayake S.M., Muthukumaran S. 2021. Effects of pavement texture and colour on Urban Heat Islands: An experimental study in tropical climate, Urban Clim.,

40, doi: 10.1016/j.uclim.2021.101024.

28. Priya U.K. and Senthil R. 2021. A review of the impact of the green landscape interventions on the urban microclimate of tropical areas, Building and Environment, 205., doi: 10.1016/j.buildenv.2021.108190.
29. Liu Y., Li Q., Yang L., Mu K., Zhang M. and Liu J. 2020. Urban heat island effects of various urban morphologies under regional climate conditions, Sci. Total Environ., 743, doi: 10.1016/j.scitotenv.2020.140589.
30. Monteiro F.F., Gonçalves W.A., Andrade L. de M.B., Villavicencio L.M.M. and dos Santos Silva C.M. 2021. Assessment of Urban Heat Islands in Brazil based on MODIS remote sensing data, Urban Clim., 35, doi: 10.1016/j.uclim.2020.100726.
31. Streutker D.R. 2002. A remote sensing study of the urban heat island of Houston, Texas, Int. J. Remote Sens., doi: 10.1080/01431160110115023.
32. Mendez-Astudillo J., Lau L., Tang Y.T. and Moore T. 2021. A new Global Navigation Satellite System (GNSS) based method for urban heat island intensity monitoring, Int. J. Appl. Earth Obs. Geoinf., 94, doi: 10.1016/j.jag.2020.102222.
33. Li H., Zhou Y., Jia G., Zhao K., Dong J. 2022. Quantifying the response of surface urban heat island to urbanization using the annual temperature cycle model. Geosci. Front., 13(1), doi: 10.1016/j.gsf.2021.101141.
34. Despini F., Ferrari C., Santunione G., Tommasone S., Muscio A.,Teggi S. 2021. Urban surfaces analysis with remote sensing data for the evaluation of UHI mitigation scenarios, Urban Clim., 35, doi: 10.1016/j.uclim.2020.100761.
35. Lucio P.S., de Toscano E.M.M., de Abreu M.L. 1999. Caracterização de séries climatológicas pontuais via análise canônica de correspondência. Estudo de caso: Belo Horizonte - MG (Brasil), Rev. Bras. Geofísica, 17(2–3), doi: 10.1590/s0102-261x1999000200008.
36. Passos R.G., Matiatos I., Monteiro L.R. Almeida R.S.S.P., Lopes N.P., Carvalho Filho C.A., Cota S.D.S. 2022. Imprints of anthropogenic air pollution sources on nitrate isotopes in precipitation in a tropical metropolitan area, Atmos. Environ., 288, 119300, doi: 10.1016/J.ATMOSENV.2022.119300.
37. de Souza D.O. and dos Santos Alvalá R.C. 2014. Observational evidence of the urban heat island of Manaus City, Brazil, Meteorol. Appl., 21(2), doi: 10.1002/met.1340.
38. de Oliveira A.P. and Fitzjarrald D.R. 1993. The Amazon river breeze and the local boundary layer: I. Observations, Boundary-Layer Meteorol., 63(1–2), doi: 10.1007/BF00705380.
39. dos S. Gomes A. C. et al. 2021 Construção de cenários futuros da temperatura máxima do ar: Capitais do Nordeste Brasileiro, Rev. Bras. Geogr. Física, doi: 10.26848/rbgf.v14.4.p2427-2445.
40. Wan Z. and Li Z.L.A. 1997. physics-based algorithm for retrieving land-surface emissivity and temperature from eos/modis data, IEEE Trans. Geosci. Remote Sens., 35(4), doi: 10.1109/36.602541.
41. Schneider A., Friedl M.A., McIver D.K., Woodcock C.E. 2003. Mapping Urban Areas by Fusing Multiple Sources of Coarse Resolution Remotely Sensed Data, Photogrammetric Engineering and Remote Sensing, 69(12)., doi: 10.14358/PERS.69.12.1377.
42. Suazo J.M.A., Rojas J.L.F., Karam H.A. 2020. Isla de Calor Urbana Superficial para Tres Megaciudades en África, Anuário do Inst. Geociências - UFRJ, doi: 10.11137/2020_2_64_75.
43. Vijith H. and Dodge-Wan D. 2020. Applicability of MODIS land cover and Enhanced Vegetation Index (EVI) for the assessment of spatial and temporal changes in strength of vegetation in tropical rainforest region of Borneo, Remote Sens. Appl. Soc. Environ., 18, doi: 10.1016/j.rsase.2020.100311.
44. Pan X., Wang Z., Gao Y., Dang X., Han Y. 2022. Detailed and automated classification of land use/land cover using machine learning algorithms in Google Earth Engine, Geocarto Int., 37(18), doi: 10.1080/10106049.2021.1917005.
45. Barat A., Parth Sarthi P., Kumar S., Kumar P., Sinha A.K. 2021. Surface Urban Heat Island (SUHI) Over Riverside Cities Along the Gangetic Plain of India, Pure Appl. Geophys., 178(4), doi: 10.1007/s00024-021-02701-6.
46. Shi H., Xian G., Auch R., Gallo K., Zhou Q. 2021. Urban heat island and its regional impacts using remotely sensed thermal data—a review of recent developments and methodology, Land, 10(8), doi: 10.3390/land10080867.
47. Chen S. Yang Y., Deng F., Zhang Y., Liu D., Liu C., Gaoet Z. 2022. A high-resolution monitoring approach of canopy urban heat island using a random forest model and multi-platform observations, Atmos. Meas. Tech., 15(3), doi: 10.5194/amt-15-735-2022.
48. Lu L., Guo H., Weng Q., Bartesaghi-Koc C., Osmond P., Li Q. 2024. A transferable approach to assessing green infrastructure types (GITs) and their effects on surface urban heat islands with multi-source geospatial data, Remote Sens. Environ., 306, doi: 10.1016/j.rse.2024.114119.
49. Venkatraman S., Kandasamy V., Rajalakshmi J., Begum S., Sujatha M. 2024. Assessment of urban heat island using remote sensing and geospatial application: A case study in Sao Paulo city, Brazil, South America, J. South Am. Earth Sci., 134, doi: 10.1016/j.jsames.2023.104763.

50. Fabrizi R., Bonafoni S., Biondi R. 2010. Satellite and ground-based sensors for the Urban Heat Island analysis in the city of Rome, Remote Sens., 2,(5), doi: 10.3390/rs2051400.
51. Shandas V., Makido Y., Upraity A.N. 2023. Evaluating Differences between Ground-Based and Satellite-Derived Measurements of Urban Heat: The Role of Land Cover Classes in Portland, Oregon and Washington, D.C., Land, 12(3), doi: 10.3390/land12030562.
52. Chongtaku T., Taparugssanagorn A., Miyazaki H.,Tsusaka T.W. 2024. Spatial-Multitemporal Analysis of Heatwaves in Thailand : Discrepancies between In-Situ Air Temperature and Remote Sensing-Derived Land Surface Temperature Spatial-Multitemporal Analysis of Heatwaves in Thailand : Discrepancies between In-Situ Air Temperature and Remote Sensing-Derived Land, doi: 10.20944/preprints202402.1324.v1.
53. Xia H., Chen Y., Song C., Li, J. Quan J., Zhou G. 2022. Analysis of surface urban heat islands based on local climate zones via spatiotemporally enhanced land surface temperature, Remote Sens. Environ., 273, doi: 10.1016/j.rse.2022.112972.
54. Janjic Z.I. 1994. The step-mountain eta coordinate model: further developments of the convection, viscous sublayer, and turbulence closure schemes, Mon. Weather Rev., 122(5), doi: 10.1175/1520-0493(1994)122<0927:TSMECM>2.0.CO;2.
55. Lim K.S.S. and Hong S.Y. 2010. Development of an effective double-moment cloud microphysics scheme with prognostic cloud condensation nuclei (CCN) for weather and climate models, Mon. Weather Rev., 138(5), doi: 10.1175/2009MWR2968.1.
56. Iacono M.J., Delamere J.S., Mlawer E.J., Shephard M.W., Clough S.A., Collins W.D. 2008. Radiative forcing by long-lived greenhouse gases: Calculations with the AER radiative transfer models, J. Geophys. Res. Atmos., 113(13), doi: 10.1029/2008JD009944.
57. Shen C., Chen X., Dai W., Li X., Wu J., Fan Q., Wang X., Zhu L., Chan P., Hang J., Fan S., Liet W. 2019. Impacts of high-resolution urban canopy parameters within the WRF model on dynamical and thermal fields over Guangzhou, China, J. Appl. Meteorol. Climatol., 58(5), doi: 10.1175/JAMC-D-18-0114.1.
58. Solano-Farias F., Ojeda M.G.V., Donaire-Montaño D., Rosa-Cánovas J.J., Castro-Díez Y. Esteban-Parra M.J., Gámiz-Fortis S.R. 2024. Assessment of physical schemes for WRF model in convection-permitting mode over southern Iberian Peninsula, Atmos. Res., 299, doi: 10.1016/j.atmosres.2023.107175.